Rolling Circle Amplification-Coupled Glass Nanopore Counting of Mild Traumatic Brain Injury-Related Salivary miRNAs

Ming Dong [†], Zifan Tang [†], Steven Hicks [‡] and Weihua Guan [*,†,§]

[†] Department of Electrical Engineering, Pennsylvania State University, University Park, Pennsylvania 16802, United States

[‡] Department of Pediatrics, Penn State College of Medicine, Hershey, Pennsylvania 17033, United States

[§] Department of Biomedical Engineering, Pennsylvania State University, University Park, Pennsylvania 16802, United States

* Corresponding Author, Email: w.guan@psu.edu, Tel: 1-814-867-5748

Contents

Supplementary Figures S2

Supplementary Table S8

Supplementary Figures

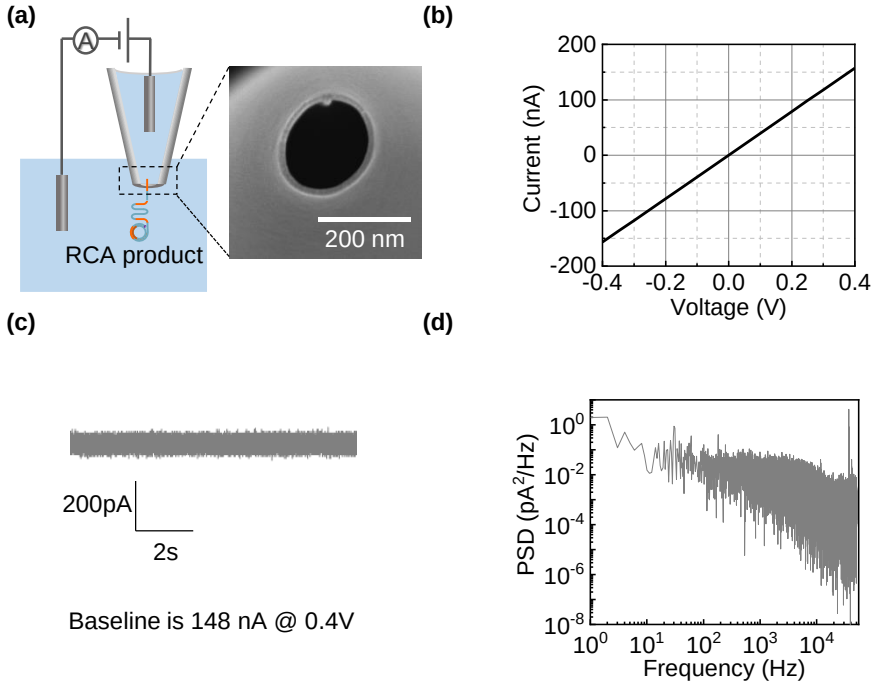


Figure S1. The experimental setup and the characterization of the glass nanopore. (a) The schematics of RCA-coupled nanopore counting setup. The enlarged SEM image shows a typical glass nanopore (~200 nm in diameter) used in our experiments. We intentionally used this large pore to avoid signals generated by small molecules like miRNAs and padlock probes. (b) IV characterization of the glass nanopore. The conductance is about 370 nS. (c) The current trace of the large glass nanopore tested in Tris-EDTA buffered 1 M KCl. (d) The power spectral density (PSD) of the current trace in (c).

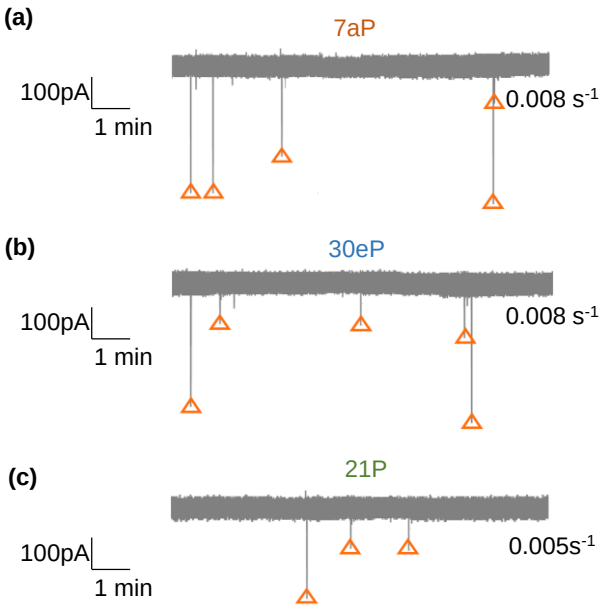


Figure S2. Current traces for the probe-only reactions for background false positive rate evaluation. (a) For 7aP probe-only reaction, 5 events captured within 10 mins (i.e., <0.008 s^{-1} false positive rate). Orange triangles annotate the captured events. (b) For 30eP probe-only reaction, 5 events captured within 10 mins (i.e., <0.008 s^{-1} false positive rate). (c) For 21P probe-only reaction, 3 events captured within 10 mins (i.e., <0.005 s^{-1} false positive rate).

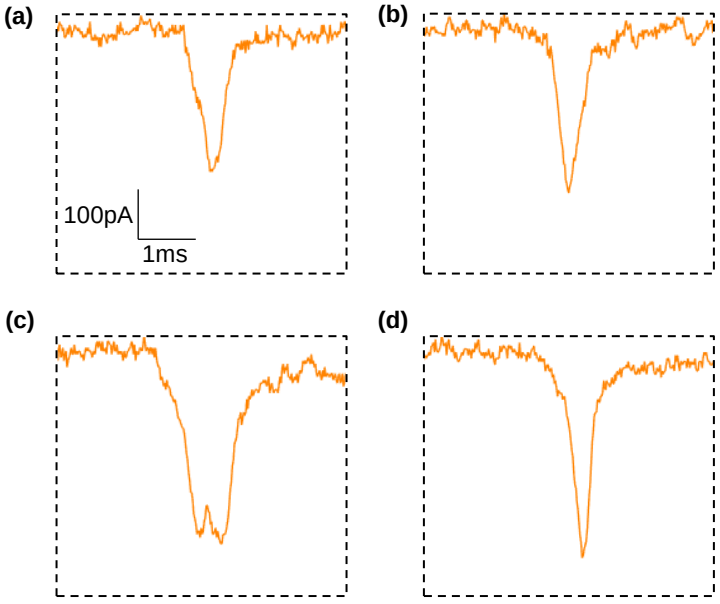


Figure S3. The typical RCA product translocation events for the let-7a panel.

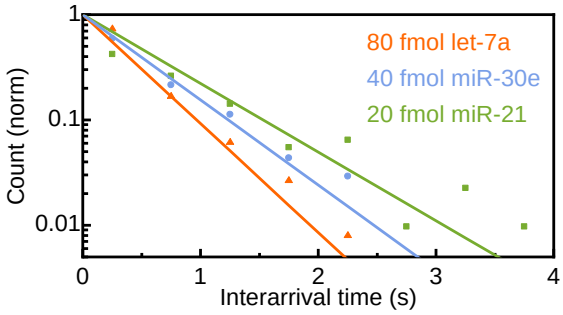


Figure S4. Normalized distributions of interarrival time for different miRNAs with monoexponential fits. The exponential distribution of the interarrival time between events indicates the translocation events follow a Poisson process, indicating the translocations are random and independent.

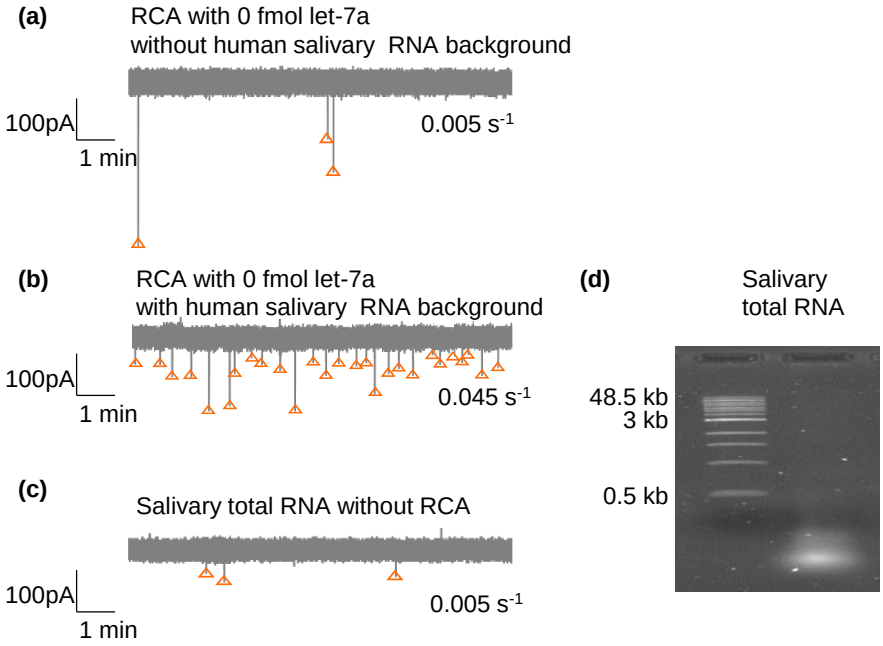


Figure S5. Evaluation of the impact of human salivary total RNA on the RCA-coupled glass nanopore counting. (a) 10 mins current trace of the 0 fmol let-7a RCA assay without total RNA background. There were only 3 events captured within 10 min of measurement time (i.e., <0.005 s^{-1} false positive rate). (b) 10 mins current trace of the 0 fmol let-7a RCA assay with total RNA background. There were 27 events captured within 10 min (i.e., 0.045 s^{-1} false positive rate). This increased background event rate is likely due to the RCA amplicons of the preexisted let-7a in the extracted salivary RNAs rather than the salivary RNAs themselves. (c) 10 mins current trace of the extracted salivary total RNA *without* RCA assay. Only three events were captured, corresponding to 0.005 s^{-1} false positive rate. This suggested the as-extracted miRNAs from saliva are too small to be effectively detected by the glass nanopores with 200 nm diameter. (d) Gel electrophoresis of extracted salivary total RNA. Most of the RNAs have a length shorter than 500 nucleotides.

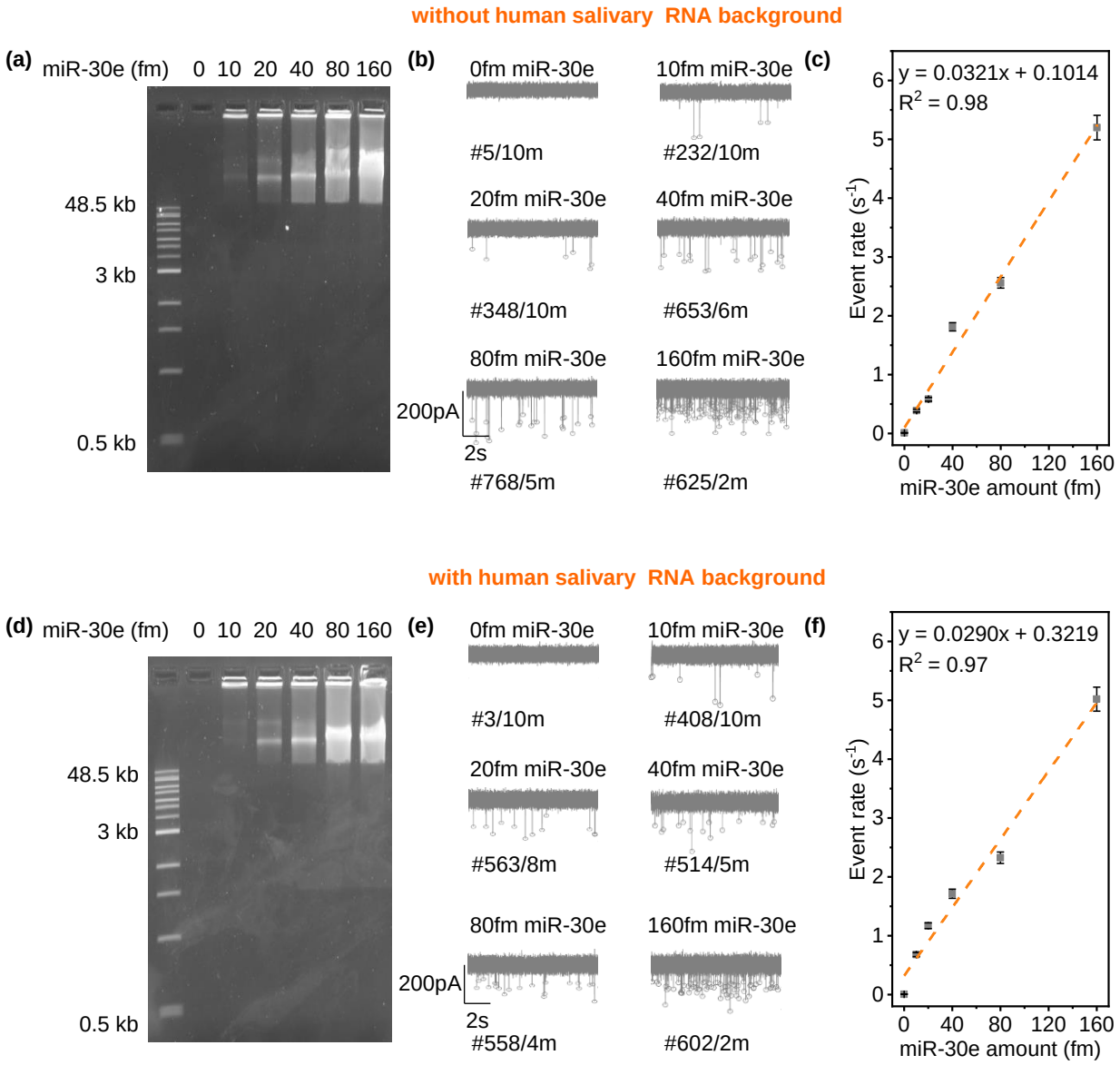


Figure S6. Quantification of miR-30e. (a) The gel image of the RCA products with different quantities of the purified miR-30e (without human salivary total RNA). (b) The corresponding current traces obtained in nanopore sensing. (c) The extracted event rate as a function of the miR-30e quantity. (d) The gel image of the RCA products with different miR-30e quantities in the salivary total RNA background. (e) The corresponding current traces obtained in nanopore sensing with salivary total RNA background. (f) The extracted nanopore event rate as a function of the miR-30e quantity with salivary total RNA background.

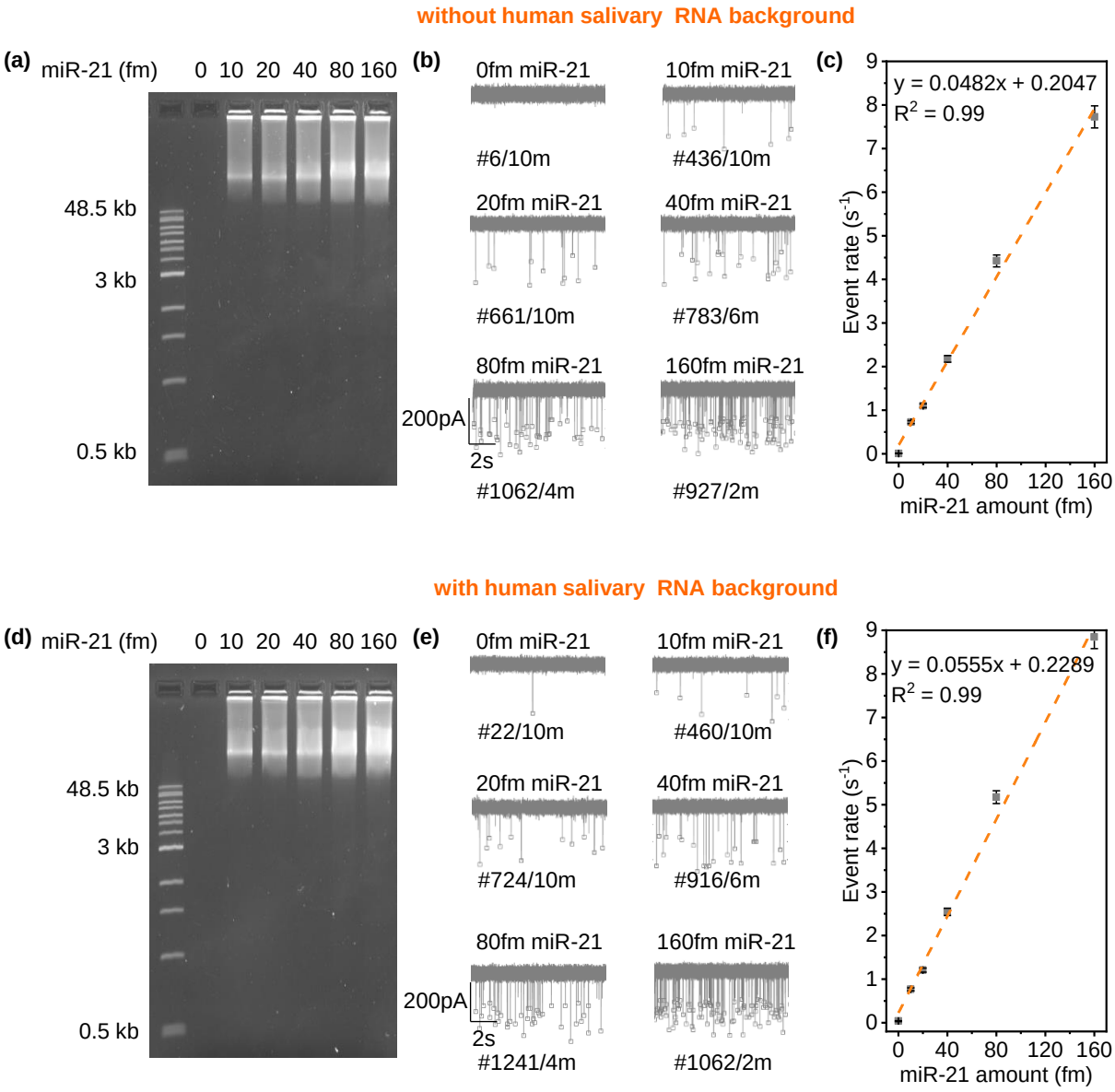


Figure S7. Quantification of miR-21. (a) The gel image of the RCA products with different quantities of the purified miR-21 (without human salivary total RNA). (b) The corresponding current traces obtained in nanopore sensing. (c) The extracted event rate as a function of the miR-21 quantity. (d) The gel image of the RCA products with different miR-21 quantities in the salivary total RNA background. (e) The corresponding current traces obtained in nanopore sensing with salivary total RNA background. (f) The extracted nanopore event rate as a function of the miR-21 quantity with salivary total RNA background.

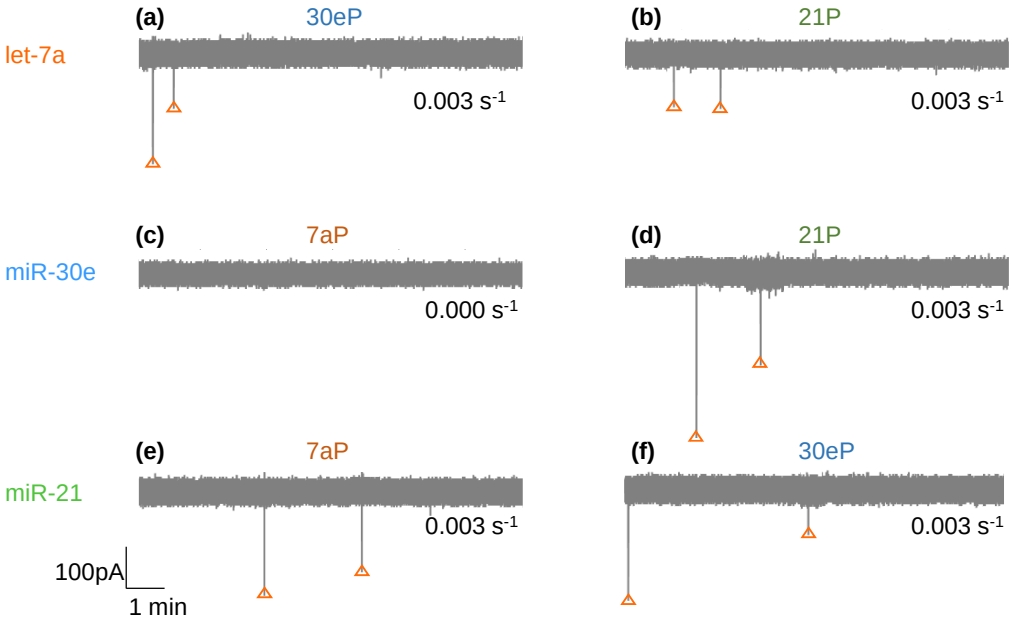


Figure S8. 10 mins current traces of the non-specific reactions. In the RCA assay, the amount of probes was fixed at 160 fmol and all miRNAs were 40 fmol. (a) let-7a RCA assay added with 30eP probe. (b) let-7a RCA assay with 21P probe added. (c) miR-30e RCA assay with 7aP probe added. (d) miR-30e RCA assay with 21P probe added. (e) miR-21 RCA assay with 7aP probe added. (f) miR-21 RCA assay with 30eP probe added. The false positive rates of all the non-specific combinations were smaller than 0.003 s^{-1}.

Supplementary Table

Table S1. miRNAs and padlock probes sequences used in this study

RNA/DNA	Sequence (5'-3')
let-7a	UGA GGU AGU AGG UUG UAU AGU U
hsa-miR-30e	UGU AAA CAU CCU UGA CUG GAA G
hsa-miR-21	UAG CUU AUC AGA CUG AUG UUG A
Padlock probe 7aP	phosphate - CTA CTA CCT CAT TTG CAT TTC AGT TTA CGG TTT AGC ATT TCG CAA TTT TAA CTA TAC AAC
Padlock probe 30eP	phosphate - GGA TGT TTA CAT TTG CAT TTC AGT TTA CGG TTT AGC ATT TCG CAA TTT TCT TCC AGT CAA
Padlock probe 21P	phosphate- CTG ATA AGC TAT TTG CAT TTC AGT TTA CGG TTT AGC ATT TCG CAA TTT TTC AAC ATC AGT

The eleven 5' (solid underlined) and 3' (dotted) terminal bases of the padlock probe were complementary to the solid underlined and dotted sequence of miRNA, respectively.